INSTITUTE OF PHYSICS PUBLISHING PHYSICS IN MEDICINE AND BIOLOGY

Phys. Med. Biol. **46** (2001) 2515–2530 PII: S0031-9155(01)24203-1

Photothermal determination of optical coefficients of tissue phantoms using an optical fibre probe

J G Laufer[1], P C Beard[1], S P Walker[2] and T N Mills[1]

[1] Department of Medical Physics & Bioengineering, University College London, London WC1E 6JA, UK
[2] Computational Mechanics Section, Mechanical Engineering Department, Imperial College, London SW7 2BX, UK

Received 23 April 2001, in final form 26 July 2001
Published 12 September 2001
Online at stacks.iop.org/PMB/46/2515

Abstract

The absorption and reduced scattering coefficients of turbid tissue phantoms have been determined from photothermal measurements made using an optical fibre probe. The thermal sensor was a thin polymer film positioned at the end of a multimode optical fibre. The film was illuminated by the output of a continuous-wave diode laser and formed the cavity of a low-finesse Fabry–Perot interferometer. Low energy laser pulses, launched into the fibre and passed through the film, produced an abrupt temperature rise in the target tissue, which was placed in contact with the film. The subsequent conduction of heat into the film caused a change in its optical thickness and hence the reflected intensity. The absorption and reduced scattering coefficients of gelatine tissue phantoms of known optical properties were determined from the measurements using a numerical model of photothermal signal generation and maximum *a posteriori* estimation. The determined optical coefficients were in good agreement with the known values. The results showed that the probe can be used for the determination of optical coefficients provided the thermal coefficients of the target tissue are known with low uncertainty.

1. Introduction

In the field of biomedical optics, pulsed photothermal techniques have been used as methods for determining the optical coefficients of tissue phantoms (Prahl *et al* 1992) and arterial tissue (Long and Deutsch 1987), measuring skin hydration (Bindra *et al* 1994) and estimating the depth of blood vessels in port wine stains (Jacques *et al* 1993). These techniques exploit the dynamics of the heating and cooling of tissue produced by pulses of optical energy and can be used to obtain information about the optical, thermal and spatial properties of the target. Most studies employ free space radiometric techniques for the detection of the photothermal response, which prohibit their application for making *in vivo* measurements deep inside the

body. There have been a number of developments in which infrared transmitting silver halide fibres were employed to guide the infrared emissions from the target to a radiometric detector (Belotserkovsky *et al* 1993, Shenfeld *et al* 1993). Such concepts could be applied to the detection of photothermal signals inside the body. However, silver halide fibres cause problems due to loss of transmittance and low damage thresholds at visible and near-infrared wavelengths. This would prohibit their use for guiding the excitation laser pulses for the measurement of the optical properties in the visible and near-infrared wavelength region. We aimed at overcoming these restrictions with the development of an optical fibre probe with a thin film Fabry–Perot interferometer as its sensing element. The film was positioned at the distal end of the optical fibre. The small size of the probe makes it suitable for minimally invasive photothermal measurements on tissue during endoscopy or for interstitial measurements. A possible application of the optical fibre probe is the *in vivo* diagnosis of carcinomas, achieved via the photothermal detection of differences in the optical coefficients of the diseased tissue compared to the normal surrounding tissue (Gandjbakhche *et al* 1995, Troy *et al* 1996). The rationale for this is that the scattering of light is usually stronger in tumours than in normal tissue (Laufer 2001). This observation may be explained by the higher content of fibres, mitochondria and the presence of enlarged nuclei. Additionally, the absorption of light in cancers is often affected by variations in the ratio of oxygenated to deoxygenated haemoglobin compared to normal tissue (Fishkin *et al* 1997). Possible differences in the thermal properties (Jain *et al* 1979, Gullino *et al* 1982) may also provide a means of identifying cancerous tissues using photothermal techniques. Our goal was to assess the potential diagnostic performance of an existing photoacoustic–photothermal optical fibre probe (Beard *et al* 1998) for the photothermal determination of the absorption coefficient, μ_a, and the reduced scattering coefficient, μ_s', of biological tissue.

The principles of operation of the optical fibre probe are discussed in section 2. In section 3, the determination of optical coefficients from experimental data using a numerical model of photothermal signal generation and maximum *a posteriori* (MAP) estimation is described. This is followed by a description of the experimental technique in section 4. The measurements of photothermal signals on non-scattering and turbid gelatine phantoms are presented and discussed in section 5.

2. The optical fibre probe

A schematic of the optical fibre probe used in this work for the generation and detection of photothermal transients in tissue is shown in figure 1. Short laser pulses are delivered to the target tissue via an optical fibre. The laser pulses are transmitted through a transparent polymer film, positioned at the distal end of the optical fibre and acting as a Fabry–Perot temperature sensor. The pulses are absorbed in the tissue where they produce an abrupt temperature rise. Heat flows into and across the sensing film, modulating its optical thickness due to thermal expansion and the temperature dependence of its refractive index.

In the absence of significant relaxation of temperature within the duration of the laser pulse and for a given sensor geometry, the spatial distribution of temperature immediately after the absorption of the pulse depends on the optical coefficients, the specific heat and the density of the tissue. The rate of the subsequent diffusion of heat through the sensing film is predominately determined by this initial temperature distribution and hence the optical coefficients, specific heat and density of the tissue, the tissue thermal conductivity and by the thermal properties of the sensing film.

The sensing film is illuminated by the output of a wavelength-tuneable diode laser delivered via the optical fibre. The Fresnel reflections due to the refractive index mismatch

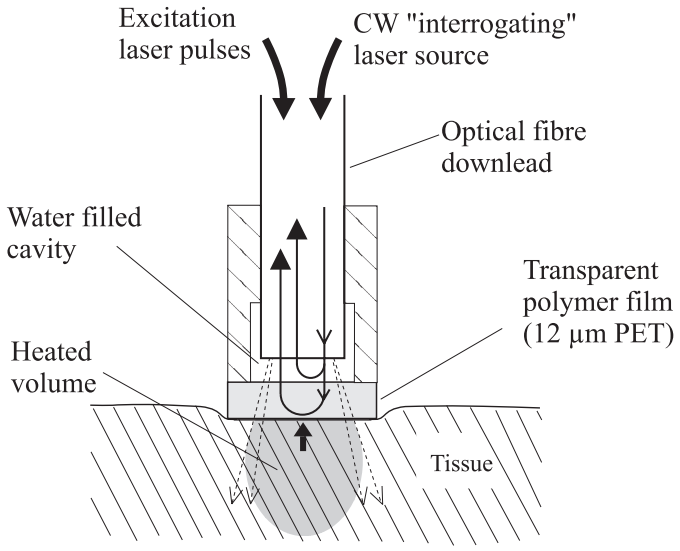

Figure 1. Schematic of the optical fibre probe for the detection of photothermal responses from tissue.

at the two faces of the film travel back along the fibre and are incident on a photodiode. The polymer film acts as a low finesse Fabry–Perot interferometer and provides a change in reflected power as a result of the thermally induced modulations in optical thickness. The phase bias of the interferometer is set to produce maximum change in reflected power per unit change in optical thickness (quadrature point) by tuning the wavelength of the diode laser. For small, thermally induced phase shifts (<0.5 rad) linear operation can be assumed. The sensing film was polyethylene terephthalate (PET) with a refractive index of $n = 1.65$. The high refractive index of PET compared to the water-based surrounding media resulted in relatively high reflection coefficients at the film boundaries, which produced high fringe visibility.

The static phase shift ϕ between the reflections from the two faces of the sensing film at normal incidence is given as

$$\phi = \frac{4\pi nl}{\lambda} \tag{1}$$

where n is the refractive index of the film material, l is the film thickness and λ is the wavelength of the light. The thermal phase sensitivity $\Delta\phi/\Delta T$ is given by

$$\frac{\Delta\phi}{\Delta T} = \frac{4\pi nl}{\lambda}\left(\frac{1}{n}\frac{\mathrm{d}n}{\mathrm{d}T} + \frac{1}{l}\frac{\mathrm{d}l}{\mathrm{d}T}\right) \tag{2}$$

where $\mathrm{d}n/\mathrm{d}T$ is the temperature coefficient of the refractive index, or thermo-optic coefficient, and $l^{-1}\mathrm{d}l/\mathrm{d}T$ is the linear thermal expansion coefficient.

Heat propagating through the film induces a change in film thickness $\mathrm{d}l$ and a change in the refractive index $\mathrm{d}n$, which give rise to a phase modulation $\Delta\phi/\Delta T$. The thermal sensitivity is therefore determined by n and l as well as their temperature coefficients. The choice of film thickness was a compromise between thermal sensitivity and detection speed. An increase in film thickness results in a higher thermal sensitivity but a longer rise time. The film thickness of 12 μm produced adequate thermal sensitivity while allowing the monitoring of fast thermal transients.

To obtain the overall system sensitivity, the thermal sensitivity is multiplied by the phase sensitivity of the interferometer, which is defined as the change in reflected intensity, ΔI_0, per unit phase shift, $\Delta\phi$. The phase sensitivity at quadrature for a low finesse cavity (Beard and Mills 1996) in which r_1 and r_2 is given by

$$\frac{\Delta I_0}{\Delta\phi} = 2I(1-r_1)\sqrt{r_1 r_2} \tag{3}$$

where I is the total incident intensity, r_1 and r_2 are the reflection coefficients of the front and rear surface of the film. The overall system sensitivity is therefore

$$\frac{\Delta I_0}{\Delta T} = \frac{8\pi n l I(1-r_1)\sqrt{r_1 r_2}}{\lambda}\left(\frac{1}{n}\frac{\mathrm{d}n}{\mathrm{d}T} + \frac{1}{l}\frac{\mathrm{d}l}{\mathrm{d}T}\right). \tag{4}$$

Equation (4) does not take into account the effects of phase dispersion caused by the divergent incident light emerging from the optical fibre and illuminating the film. This neglect is reasonable due to the very small cavity thickness and low beam divergence ($<3.5^\circ$) (Pérennès *et al* 1999).

3. The numerical model of photothermal signal generation

A model for the prediction of photothermal signals was developed for the determination of the optical and thermal coefficients of tissue phantoms from detected photothermal signals. The coefficients were determined by fitting the model to signals using MAP estimation. The numerical model of the photothermal signal generation was a combination of models of light transport, which provided the initial temperature distribution, and a finite element model (FEM), which was used to calculate the time-varying heat transfer through the sensing film.

Studies employing radiometric techniques typically use analytic theories to describe the time-course of the photothermal signal. This requires a number of simplifying approximations in order to describe adequately the heat transport in the target. One approximation is that heat flows in only one spatial direction, which allows analytical solutions to the heat conduction equation to be obtained more easily. This approach is justified when radiometric techniques are configured such that a one-dimensional thermal geometry is obtained. This can achieved by using a small area of photothermal detection at the centre of a large area of excitation. The optical fibre probe, however, requires the modelling of transient heat conduction in two dimensions since it produces both axial and radial heat flow. Numerical techniques such as the method of finite elements, which was employed here, provide the ability to model heat flow in objects of arbitrary geometry with spatially varying thermal properties. Finite element models can provide a numerical solution to the heat conduction equation, which is solved between the individual nodes of a mesh using shape functions. It is important to bear in mind that finite elements only provide approximate solutions to the heat conduction equation. This limitation can be taken into account by reducing the inter-nodal distance in the finite element mesh and thereby letting the FEM converge to the true solution.

The geometrical model for transient heat conduction in the optical fibre probe and the tissue was created using Patran (MSC Software). The model comprised an axially symmetric two-dimensional cross-section of the optical fibre probe and the adjacent target tissue as illustrated in figure 2. The thermal properties of the sensor materials and tissue were distributed across the finite element mesh according to their dimensions and were assumed to be unaffected by temperature changes. The thermal constants of tissue were set to those of water. The interface between the film and the surrounding media was assumed to be thermally continuous. The mesh boundaries were located far from the area of photothermal signal generation. This ensured that the boundary conditions did not influence the solution in the region of the mesh

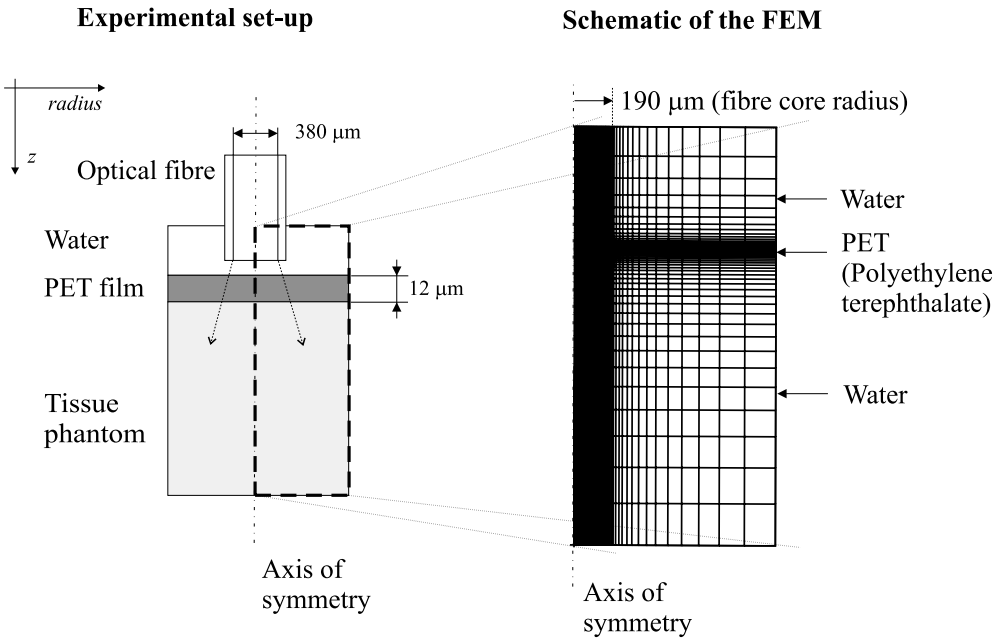

Figure 2. Representation of the experimental configuration of the optical fibre probe in the finite element model of heat transport. The dark area of the mesh illustrates a high node density across the sensing film and the adjacent tissue.

used for calculating the photothermal signal during the period of interest. The element spacing of the mesh across the sensing film and the adjacent tissue was sufficiently small to allow the accurate simulation of photothermal responses for typical tissue optical coefficients. A separate programme (Abaqus®) was employed to calculate the transient heat conduction using the FEM.

The light distribution caused by a laser pulse was calculated using the Lambert–Bouguer law for purely absorbing targets. For turbid tissue phantoms, an existing Monte Carlo model (Wang *et al* 1995, 1997) was modified to compute the spatial distribution of absorbed optical energy produced by a divergent beam of Gaussian fluence profile in a semi-infinite slab with absorbing and scattering properties. The distribution of absorbed optical energy obtained from the relevant light transport model was converted to a temperature distribution, which was then incorporated as an initial condition into the FEM of transient heat conduction. The FEM calculated the temperature profiles in the finite element mesh for a number of discrete time increments. The theoretical photothermal signal, which is equivalent to the time-variant change in the optical thickness of the Fabry–Perot cavity, was obtained by integrating the temperature distributions in the film across the film thickness and the area of optical detection for each time increment. In practice, the signal amplitude incorporated an additional scaling parameter, the calibration constant, which represented the overall sensitivity of the system and the pulse energy.

3.1. Determination of optical coefficients from experimental data using MAP estimation

The aim of the work described in this paper was to determine the absorption and scattering coefficients of tissues from photothermal signals detected using the optical fibre probe. The

optical coefficients were obtained indirectly from the interferometric measurement of thermally induced thickness changes of the sensing film. In view of the envisaged application, it was particularly important to address the effects of possible variations in the thermal coefficients of tissue on the accuracy with which the optical coefficients could be determined. This was necessary since the photothermal response of tissue is determined by both the optical and thermal properties of the tissue. One of the options for obtaining coefficients from photothermal signals is the minimization of the difference between experimental observation and model prediction, also known as chi-square minimization. However, such an approach takes no account of the uncertainties in the experiment and the parameters used in the model and does not provide an insight as to whether more than one set of parameters is able to predict a photothermal measurement to within experimental and modelling uncertainties. MAP estimation (Beck and Arnold 1977) addresses such multi-parameter problems and provides a statistical tool for the extraction of model parameters from experimental data. MAP estimation was applied to determine the optical and thermal coefficients by minimizing the difference between the experimental data and the model predictions incorporating any prior knowledge of the coefficients and the experimental error. Prior knowledge based on values reported in the literature was incorporated in the form of mean values and uncertainties in the optical and thermal coefficients of tissue. Experimental uncertainties were incorporated as standard deviations of repeated measurements. Through the comparison of the uncertainties before and after the determination of the optical and thermal coefficients, MAP estimation also provided a means of quantifying the improvement in the knowledge of the optical coefficients that was gained by fitting the model to the data. The estimated uncertainties in the parameters of interest, μ_a and μ_s', were calculated not only on the basis of the improvement of the fit but also by taking into account the uncertainties of all other model parameters such as the thermal conductivity, k, specific heat, c, and density, ρ.

MAP estimation of the optical coefficients required the linearization of the FEM around a set of parameters β, which included μ_a, μ_s', k, c, ρ and the calibration constant. Uncertainties in other model parameters such as the physical properties of the polymer film were found to introduce negligible uncertainties to the photothermal signal. The linear output of the model or 'theoretical signal' is defined as η and can be calculated using

$$\eta = X\beta \tag{5}$$

where $X = \mathrm{d}S_{\mathrm{np}}/\mathrm{d}c_{\mathrm{p}}$ is the so-called design matrix, which contains the derivatives of each point of the model prediction, S_{np}, with respect to the parameters c_{p} contained in β. η is a vector of the n data points of the photothermal signal. X is a $[n \times p]$ matrix and β is a vector of the p parameters. The vector of coefficients that produce minimum discrepancy between the experimental data and the model, b_{MAP}, were obtained using equation (6). For a derivation of equation (6) the reader is referred to a publication by Beck and Arnold (1977). The values of the estimated parameters, b_{MAP}, were dependent upon the initial parameters contained in μ_β, the vector of the photothermal signal, Y, the $[p \times p]$ matrix of the covariance or initial uncertainty of the parameters, V_β, and the $[n \times n]$ covariance matrix of the measurement errors, ψ, using

$$b_{\mathrm{MAP}} = \mu_\beta + P_{\mathrm{MAP}}\, X^{\mathrm{T}}\psi^{-1}(\mathrm{Y} - X\mu_\beta) \tag{6}$$

with

$$P_{\mathrm{MAP}} = \left(X^{\mathrm{T}}\psi^{-1}X + V_\beta^{-1}\right)^{-1}. \tag{7}$$

Owing to the linearization of the numerical model, the minimization of the difference between the photothermal signals and the numerical model could in theory be achieved in a single step

using equation (6). However, the linearization is of course only valid for small variations in the model parameters. To take account of the growing divergence between the linearized model of equation (5) and the FEM, the so-called predictor–corrector method was employed for the minimization procedure. One step of the predictor–corrector method in the minimization procedure involved a number of calculations including the computation of the design matrix around the initial parameter values, the estimation of the new set of parameters and the calculation of a second design matrix for the new set of parameters. Finally, the mean of the two design matrices was used to determine the new parameters from the set of initial parameters. It was generally found that MAP estimation needed be repeated only three times to achieve the convergence criterion of a change in residuals of less than 1 part in 5000. The set of parameters that produced the closest match to the data was selected as the final result of the estimation.

The uncertainties of the new parameters were calculated using (Beck and Arnold 1977)

$$\mathrm{cov}(b_{\mathrm{MAP}} - \beta) = P_{\mathrm{MAP}} = \left(X^{\mathrm{T}}\psi^{-1}X + V_{\beta}^{-1}\right)^{-1}. \tag{8}$$

The estimated parameter covariance given by equation (8) is an important value, since it represents the degree by which our knowledge of the parameters has increased through using MAP estimation. For example, if the final uncertainty of a parameter is large and has not been reduced significantly compared to the initial uncertainty, it implies that any other parameter value within the boundaries of the uncertainty would produce similar agreement with the measurement. The final value of the coefficient is then of small importance and the insignificant reduction of the initial uncertainty suggests that the knowledge in the coefficient has not been increased.

For the determination of μ_{a} from photothermal measurements on non-scattering tissue phantoms, the initial values of the thermal coefficients were assumed to be those of water since it is the largest constituent of the tissue phantoms. The initial uncertainties were chosen to be $\pm 1\%$. The μ_{a} and the calibration constant were assigned large initial uncertainties of e.g. $\pm 50\%$. The estimation procedure was similar to that suggested by Prahl *et al* (1992) who found that a two-parameter fit provides the most accurate method of determining μ_{a} and the calibration constant from the photothermal signal.

The calibration constant and the thermal coefficients were implemented as a fixed parameter by setting the prior uncertainty to $\pm 1\%$ in the estimation of μ_{a} and μ_{s}' from measurements on turbid tissue phantoms. This was necessary because the estimation procedure would not yield meaningful results from a photothermal signal if both the optical and thermal coefficients are included as 'unknown' parameters (Prahl *et al* 1992).

4. Experimental technique

4.1. Experimental set-up

The sensing element of the optical fibre probe consisted of a 12 μm transparent polymer film mounted in front of the distal end of an optical fibre of low numerical aperture (NA $= 0.12$) as shown in figure 3.

The film was illuminated by the coherent output of a wavelength-tuneable diode laser (774–794 nm, 11 mW, Newport Inc.). The Fresnel reflections caused by the refractive index mismatch between the sensing film and the adjacent media travelled back along the fibre and were incident on a photodiode (0.5 mm^2, 15 MHz, Hamamatsu S6468) for detection. The polymer film acted as a low finesse Fabry–Perot interferometer, which produces an approximately linear change in the reflected power for small measurand-induced variations in

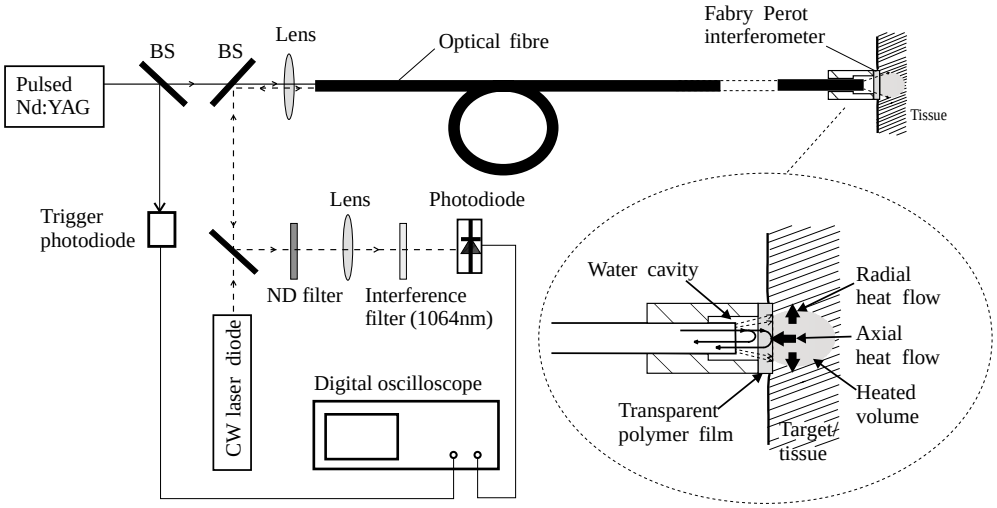

Figure 3. Experimental configuration of the optical fibre probe.

the optical thickness. This required the interferometer to be operated at the so-called point of quadrature obtained by tuning the laser wavelength, which resulted in a maximum change in reflected power per unit phase shift. A fixed-Q Nd:YAG laser (InnoLas Ltd., UK) was used to provide excitation pulses (200 μs, 0.02–0.04 J mm^{-2}) at 1064 nm. The excitation pulses were transmitted through the sensing film and absorbed in the target, which produced an abrupt temperature rise. The subsequent heat flow into the film modulated its optical thickness due to the temperature dependence of its thickness and refractive index. Since the fastest rise times of the photothermal signals were of the order of 150 μs, the effective bandwidth was limited to 10 kHz with an active low-pass Butterworth filter to improve the noise characteristics of the system. To prevent saturation by the excitation light, a 1064 nm interference filter was placed in front of the photodiode. A 200 MHz digital oscilloscope (Tektronix TDS 360) was used to record the signals. The dc thermal sensitivity was measured by monitoring the probe output while it was placed in a water bath, which cooled from 55 °C to ambient temperatures. A thermal noise floor of 250 mK was calculated from the thermal sensitivity and the typical noise voltage that is produced by the photodiode and the amplifier for a bandwidth of 10 kHz. The thermal phase sensitivity (equation (2)) was measured as 0.02 rad K^{-1}.

4.2. Tissue phantoms

Water-based tissue phantoms of known optical coefficients were made using gelatine, a near-infrared molecular dye (Zeneca, S109564) and polystyrene microspheres (B Harness, Department of Chemical Engineering, University of Bradford). The absorption coefficients of solutions of distilled water and dye at 1064 nm were determined from the measurement of their transmittance at this wavelength.

During preliminary measurements on gels containing the absorbing dye without added scatterers, it was found that a thin layer of dye was deposited onto the sensing film, which resulted in significant errors. To avoid the contamination of the film, a small amount of polystyrene microspheres were mixed into the gels to immobilize the dye. Calculations using the Monte Carlo model confirmed that the light distribution in the gels with such a small amount of added scatterers could be approximated using the Lambert–Bouguer law with

adequate accuracy. These gels, which have a $\mu_s' = 0.2\,\mathrm{mm}^{-1}$, are referred to as non-scattering phantoms for the remainder of this paper. By varying the concentration of the dye in the gels, phantoms with μ_a ranging from 0.5 to 3.1 mm^{-1} were made.

Scattering was introduced by adding polystyrene microspheres. The scattering coefficient depended upon the volume fraction of the spheres in the liquid and their size distribution. The reduced scattering coefficient, $\mu_s' = \mu_s(1-g)$, and the scattering anisotropy, g, were calculated using Mie theory (Kohl *et al* 1995). The suspension was placed in an ultrasonic bath for 30 min to minimize lumping of the scattering particles. A small, fixed percentage of gelatine was mixed into the turbid liquid, which was then heated to approximately 40 °C and placed in a refrigerator to set. The absorption coefficient of the turbid phantoms ranged from 0.54 to 3.14 mm^{-1}, while the reduced scattering coefficient varied from 0.2 to 2.2 mm^{-1}. For all phantoms with a $\mu_s' > 0.2$ mm^{-1}, the Monte Carlo model was employed to calculate the distribution of absorbed optical energy.

4.3. Experimental methods

The gelatine tissue phantoms were cut into cubes of about 6 mm in width using a scalpel. This produced flat surfaces for good thermal contact between the sensing film and the tissue phantom. Single laser pulses were launched into the optical fibre to generate a photothermal response in the sample. The pulses were repeated at a rate of repetition of less than 0.2 Hz to prevent a shift in the baseline temperature and melting of the gels. The measurements were recorded on a digital oscilloscope and the signals were averaged over 32 acquisitions. Two measurements were made at different places on each of a total of five different samples, which were taken from a range of different depths of each tissue phantom to minimize the effects of sedimentation of the scatters. The amplitudes of the excitation laser pulses were monitored by the trigger photodiode and were later used to normalize the photothermal signals. The signals detected in a tissue phantom were normalized by the incident pulse energy and the standard deviation (10 measurements per tissue phantom) was calculated. The signal was reduced to 200 data points between 0.2 ms and 40 ms in increments of 0.2 ms.

5. Results and discussion

The optical coefficients were determined using MAP estimation as described in section 3.1. The measurements on non-scattering gelatine samples were used to assess the validity of the numerical model and to determine the calibration constant, which was then used for the estimation of the absorption and reduced scattering coefficients of turbid tissue samples.

5.1. Non-scattering phantoms

Figure 4 illustrates the effect of μ_a on the detected photothermal signals, which were normalized to the signal peak. The effect of an increase in the absorption coefficient is a more rapid decay of the photothermal signal. The signal detected in the phantom with the highest μ_a exhibits the fastest decay. An increase in μ_a results in shorter optical penetration depths and in a larger temperature gradient across the sensing film. This contributes to a more rapid heat flow through the sensing film and a faster decay of the detected photothermal response.

Figure 5 shows good agreement between the model's predictions and a photothermal signal detected in a non-scattering tissue phantom. The absorption coefficient and the calibration constant were obtained for the initial parameters and uncertainties shown in table 1.

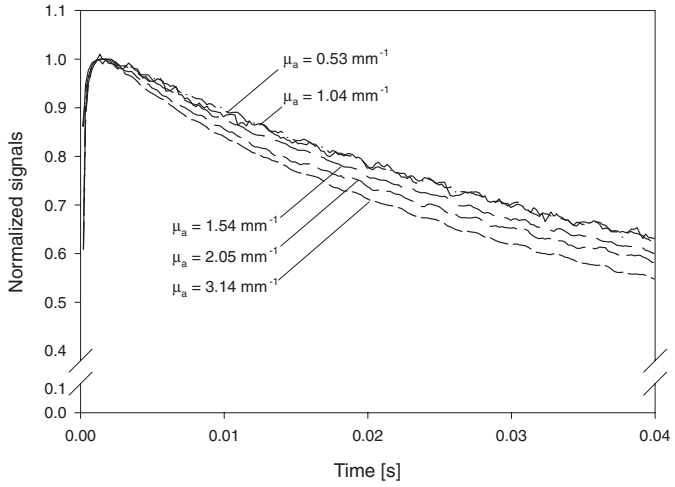

Figure 4. Normalized photothermal signals detected using the optical fibre probe on non-scattering gels with absorption coefficients ranging from 0.53 to 3.14 mm^{-1}.

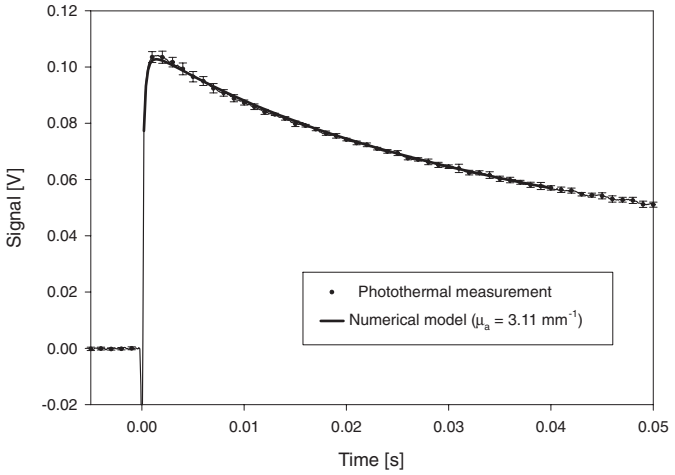

Figure 5. Comparison of the signal calculated using the coefficients obtained through MAP estimation listed in table 2 and the experimental data for a non-scattering phantom with a 'true' $\mu_{\text{a}} = 3.14\ \text{mm}^{-1}$. The error bars represent the standard deviation of 10 measurements. The absorption coefficient was obtained using small initial uncertainties in the thermal parameters.

Table 1 shows that the large initial uncertainties in the absorption coefficient and the calibration constant were greatly reduced by MAP estimation. The absorption coefficients that were determined from measurements on the remaining non-scattering gels are listed in table 2.

The good agreement between the numerical model and the experimental observations over a large range of μ_{a} served as a validation of the numerical model of photothermal signal generation. Based on this validation it was concluded that the Lambert–Bouguer law could be exchanged with an existing Monte Carlo model (Wang *et al* 1995, 1997) to calculate the distribution of absorbed optical in turbid tissue phantoms.

Table 1. Initial and determined parameters and uncertainties obtained from a photothermal measurement on a non-scattering tissue phantom with a 'known' $\mu_a = 3.14\ mm^{-1}$ using MAP estimation. The initial uncertainties in the thermal coefficients were small, which produced a determined μ_a close to the true value.

Parameter	'Known' value	Initial value ± uncertainty	Determined value ± uncertainty
μ_a (mm^{-1})	3.14	2.60 ± 1.00	3.11 ± 0.03
Calibration constant	–	0.10 ± 0.02	0.100 ± 0.001
k ($W\ mm^{-1}\ K^{-1}$)	0.56×10^{-3}	$0.56 \times 10^{-3} \pm 5.60 \times 10^{-6}$	$0.55 \times 10^{-3} \pm 4.00 \times 10^{-6}$
c ($J\ g^{-1}\ K^{-1}$)	4.18	4.18 ± 0.04	4.160 ± 0.037
ρ ($g\ mm^{-3}$)	1.0×10^{-3}	$1.0 \times 10^{-3} \pm 20.0 \times 10^{-6}$	$0.98 \times 10^{-3} \pm 14.0 \times 10^{-6}$

Table 2. Absorption coefficients obtained from photothermal measurements on non-scattering gels using small initial uncertainties in the thermal coefficients.

'Known' μ_a (mm^{-1})	Initial μ_a ± uncertainty (mm^{-1})	Determined μ_a ± uncertainty (mm^{-1})
0.53	0.53 ± 0.2	0.55 ± 0.01
1.04	0.70 ± 1.0	1.00 ± 0.03
1.57	1.30 ± 0.7	1.54 ± 0.02
2.05	1.70 ± 1.0	2.08 ± 0.03
3.14	2.60 ± 1.0	3.11 ± 0.03

Table 3. Initial and determined parameters and uncertainties obtained from a photothermal measurement ($\mu_a = 3.14\ mm^{-1}$). The initial uncertainties in the thermal coefficients were comparable to those of tissue. Note the strong deviation of all parameters from the 'known' values and the smaller reduction in the final uncertainties.

Parameter	'Known' value	Initial value ± uncertainty	Determined value ± uncertainty
μ_a (mm^{-1})	3.14	2.60 ± 1.00	3.12 ± 0.27
Calibration constant	–	0.10 ± 0.02	0.085 ± 0.005
k ($W\ mm^{-1}\ K^{-1}$)	0.56×10^{-3}	$0.56 \times 10^{-3} \pm 56.0 \times 10^{-6}$	$0.33 \times 10^{-3} \pm 6.00 \times 10^{-6}$
c ($J\ g^{-1}\ K^{-1}$)	4.18	4.18 ± 0.67	2.69 ± 0.19
ρ ($g\ mm^{-3}$)	1.0×10^{-3}	$1.00 \times 10^{-3} \pm 0.05 \times 10^{-3}$	$1.01 \times 10^{-3} \pm 0.04 \times 10^{-3}$

The significant reduction in the uncertainties of the determined absorption coefficients demonstrates that the knowledge and confidence in the estimated μ_a and calibration constant were greatly improved as a result of the estimation. However, the good agreement between the determined μ_a and the 'known' values depends, amongst other factors, upon the small initial uncertainties with which the thermal coefficients entered MAP estimation. Since the thermal properties were effectively frozen to within ±1%, it was assumed that the amplitude and shape of the photothermal signal was solely the result of the absorption coefficient and the calibration constant. While it is valid to regard the thermal properties of tissue phantoms as known to within a small uncertainty, this may not be an adequate assumption for the thermal coefficients of biological tissue. The thermal properties of tissues are determined by their composition and exhibit a greater uncertainty than tissue phantoms. In order to examine the effect of larger uncertainties in the thermal coefficients on the accuracy of the obtained μ_a, MAP estimation was repeated on the experimental data obtained from a gel with $\mu_a = 3.14\ mm^{-1}$ (figure 5). The uncertainties of the thermal conductivity, specific heat and density used in MAP estimation were representative of the upper end of uncertainties found in tissue (Duck 1990, Valvano *et al* 1985, Bowman 1981). The results are shown in table 3.

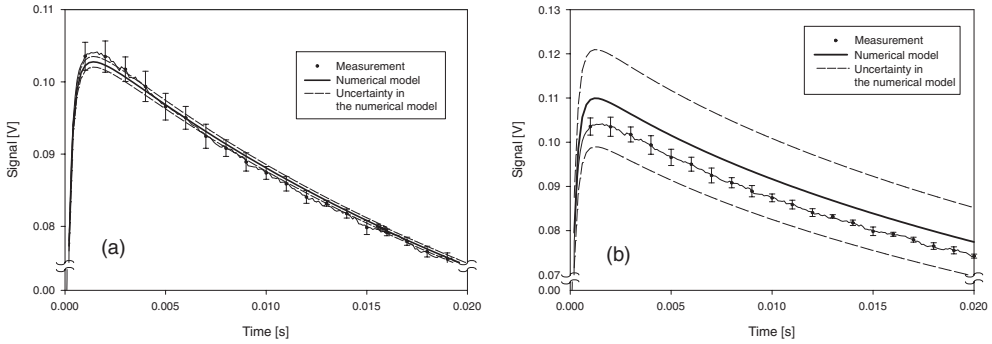

Figure 6. Comparison of a photothermal signal ($\mu_a = 3.14\ \text{mm}^{-1}$) with the model data obtained using the determined sets of parameters and their uncertainties. The results of table 1 produced an uncertainty in the model within the experimental error shown in graph (a). The results obtained using large initial parameter uncertainties (table 3) produced a large uncertainty in the FEM and an unsatisfactory agreement with the data shown in graph (b).

While the determined absorption coefficient shown in table 3 is close to the 'known' μ_a, the determined thermal coefficients are very different from the true values. The uncertainties of all coefficients have also not been reduced as strongly as during the calculations with small initial uncertainties. This indicates, for example, that any other value of μ_a within the relatively large final uncertainty would have produced a similarly good agreement with the experimental data. The results shown in table 3 can be visualized by calculating the standard deviation in the theoretical signals. The standard deviation was obtained from the variation in the theoretical signals calculated for all determined coefficients with added and subtracted uncertainties.

Figure 6(a) shows that the standard deviation of the theoretical signals calculated from the determined coefficients for the case of thermal coefficients with low prior uncertainty falls within the experimental error. This also produces good agreement between the model and the photothermal signal. Figure 6(b) illustrates the effects of large initial uncertainties on the standard deviation of the model predictions. The uncertainty in the model is much greater than the experimental error. For the determination of meaningful optical coefficients, therefore, it is essential that the thermal coefficients of tissue are of low uncertainty. In view of these results, the thermal coefficients were fixed for the determination of the μ_a and μ_s' from measurements on turbid gelatine samples which is discussed in the next section.

5.2. Turbid tissue phantoms

The measurements on turbid phantoms were investigated to assess the sensitivity of the probe to variations in the reduced scattering coefficient found in tissue. The absorption coefficient was the same for all three gels at $\mu_a = 2.05\ \text{mm}^{-1}$, while the reduced scattering coefficient was different (0.2, 1.22, 2.2 mm^{-1}). The measurements shown in figure 7 illustrate that the effect of an increase in the reduced scattering coefficient manifests itself as a small increase in the signal amplitude. The shape of the signal is not affected significantly.

The optical coefficients were obtained using MAP estimation using the calibration constant obtained from measurements on non-scattering gels (section 5.1) and the thermal coefficients by setting their initial uncertainties to $\pm 1.0\%$. The absorption and reduced scattering coefficient were given large uncertainties. The calibration constant was normalized by the

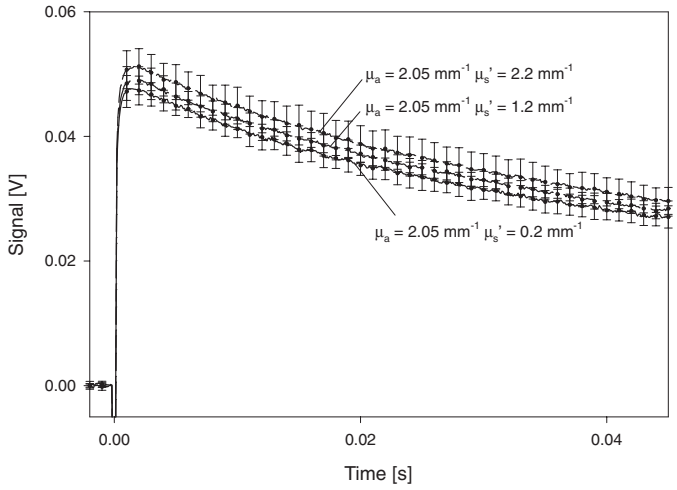

Figure 7. Photothermal signals detected in turbid gels using the optical fibre probe. The absorption coefficient was 2.05 mm^{-1} in all samples, while the reduced scattering coefficient ranged from 0.2 to 2.2 mm^{-1}. The increase in the scattering coefficient raises the amplitude of the photothermal signal but does not produce a significant change in its shape.

Table 4. Inital absorption and reduced scattering coefficients, their uncertainties and the determined values and uncertainties obtained from the photothermal responses detected in turbid tissue phantoms using MBPE.

μ_a (mm^{-1}) 'known'	μ_a (mm^{-1}) initial	μ_a (mm^{-1}) estimated	μ_s' (mm^{-1}) 'known'	μ_s' (mm^{-1}) initial	μ_s' (mm^{-1}) estimated
2.05	1.7 ± 1.0	2.08 ± 0.03	0.2	0.2 ± 0.1	0.12 ± 0.08
2.05	1.7 ± 1.0	2.08 ± 0.03	1.2	1.0 ± 0.5	1.44 ± 0.14
2.05	1.7 ± 1.0	1.89 ± 0.08	2.2	1.7 ± 0.5	2.76 ± 0.44

pulse energies and the values of the thermal coefficients, which have so far been assumed to be those of water, were adjusted to take account of the volume fraction of polystyrene microspheres. For example, the maximum volume fraction of 5%, which produced $\mu_s' = 2.2\ \mathrm{mm}^{-1}$, resulted in $k = 0.95 \cdot k_{\mathrm{water}} + 0.05 \cdot k_{\mathrm{polystyrene}} = 0.54 \times 10^{-3}\,\mathrm{W\,mm^{-1}\,K^{-1}}$. The change in the thermal coefficients due to the polystyrene microspheres was very small and did not affect the shape of the photothermal signal because the thermal diffusivity ($\alpha = k\ c^{-1}\ \rho^{-1}$) did not change significantly. Only the amplitude of the signal was affected by the variation in the specific heat capacity, which resulted in a slightly higher initial temperature. Table 4 shows the absorption and reduced scattering coefficients obtained from the measurements presented in figure 7.

The estimated values of μ_a and μ_s' shown in table 4 are close to the 'known' values. The estimated uncertainties of μ_a are generally much smaller than their starting value while the final uncertainties of μ_s' have been reduced to a lesser extent. The final uncertainties indicate that the photothermal signal has a much lower sensitivity to μ_s' compared to that of μ_a. The estimated parameters and their uncertainties demonstrate that μ_a and μ_s' can be determined from the photothermal response of turbid gels. One should bear in mind, however, that the μ_s' was determined on the basis of small differences in signal amplitude which could

also be brought about by variations in the specific heat and the density of the target. It is therefore essential that the thermal coefficients are known beforehand if μ_s' is to be determined accurately. If the thermal coefficients enter the estimation procedure with a high degree of uncertainty, no meaningful values for μ_a and μ_s' can be obtained. Similarly, variations in the calibration constant due to changes in the detector sensitivity can also have an effect on the accuracy of the determined optical coefficients.

The insensitivity of the shape of the photothermal signal to changes in the reduced scattering coefficient is due to the less-pronounced effect of μ_s' compared to μ_a on the distribution of the deposited optical energy. For tissue-like media where $\mu_a \ll \mu_s'$, this can be illustrated by calculating the optical penetration depth, δ, which is defined as $\delta = (3\mu_a(\mu_a + \mu_s'))^{-1/2}$ and, as was discussed in section 4.3, is related to the decay time of the photothermal signal. For example, the change in δ due to a change in μ_a by a few percent is much greater than that produced by an equal change in μ_s'. Photothermal techniques such as the optical fibre probe are therefore better suited to the photothermal detection of differences in the absorption coefficient than the reduced scattering coefficient.

6. Conclusions

The results have shown that the absorption and reduced scattering coefficient can be determined from photothermal signals detected in tissue phantoms using the optical fibre probe. The experimental results have demonstrated that the change in the photothermal response is a relatively weak indicator of changes in μ_s'. It was also found that the accuracy of μ_a and μ_s' is dependent upon the uncertainty in the thermal coefficients. For typical variations in the thermal properties of certain different tissue types, the optical coefficients could not be determined with adequate accuracy. Photothermal techniques in general require one of the two groups of coefficients, either optical or thermal properties, to be known with low uncertainty in order to be able to determine the other. However, the variations in the thermal properties of particular tissues may not be as large as was assumed above and for those photothermal techniques may be applicable. Nevertheless, the thermal coefficients of tissue may always need to be measured beforehand in order to obtain maximum accuracy in the tissue optical coefficients from photothermal signals.

This might be achieved by determining the thermal coefficients from photothermal signals that were generated using an excitation wavelength at which the optical properties of tissue are constant. This represents a reversal of the approach described in this paper in that one would assume that the optical coefficients are known in order to obtain the thermal coefficients. The measurement of the thermal coefficients may be achieved by using excitation wavelengths where water is highly absorbing (e.g. 1.44 μm, 2.1 μm and 2.94 μm). The effects of optical scattering would also be much smaller at these wavelengths compared to the visible and near-infrared region. Provided the optical coefficients of tissue can be approximated by the μ_a of water, and scattering can be regarded as constant or even negligible, the photothermal response detected by the optical fibre probe could be used to determine the thermal coefficients of the tissue. The thermal coefficients obtained this way could then be used for the determination of tissue optical coefficients from separate measurements at excitation wavelengths of interest in the visible or near-infrared wavelength spectrum. This approach could be simplified if the detection of differences in the optical coefficients rather than absolute values is of interest. The photothermal signals generated in the tissues using infrared excitation wavelengths could be compared to identify differences in the thermal properties. If there are negligible variations between these signals, the photothermal responses at visible or near-infrared wavelengths

could then be compared directly. Any differences in the signals would be due to differences in the optical properties.

If these assumptions hold true, the optical fibre probe could be applied to *in vivo* measurements of the optical and thermal properties of tissue located deep inside the body and accessed endoscopically or interstitially. The optical fibre probe could also be applied to photothermal imaging by using an array of sensors. This would allow a direct comparison between simultaneous measurements detected by different parts of the array without the need to normalize, which would allow a direct indication of differences in the optical and thermal properties of different areas of the target tissue.

Acknowledgments

The authors acknowledge the support of the Engineering and Physical Sciences Research Council (EPSRC) which funded this project and also thank Mike Bluck at Imperial College London for his help in the development of the numerical model.

References

Beck J V and Arnold K J 1977 *Parameter Estimation in Engineering and Science* (New York: Wiley)

Beard P C, Pérennès F, Draguioti E and Mills T N 1998 Optical fibre photoacoustic–photothermal probe *Opt. Lett.* **23** 1235–7

Beard P C and Mills T N 1996 Extrinsic optical-fibre ultrasound sensor using a thin polymer film as a low-finesse Fabry–Perot interferometer *Appl. Opt.* **35** 663–75

Belotserkovsky E, Mesh M, Shlifer A, Eyal A and Katzir A 1993 IR fibreoptic radiometric thermometry for biomedical applications *Proc SPIE* **2085** 109–14

Bindra R M S, Imhof R E, Mochan A and Eccleston G M 1994 Opto-thermal technique for *in vivo* stratum corneum hydration measurement *J. Physique* IV Colloque C7, supplément au Journal de Physique III **4**

Bowman H F 1981 Heat transfer and thermal dosimetry *J. Microwave Power* **16** 121–33

Duck F A 1990 *Physical Properties of Tissue: A Comprehensive Reference Book* (San Diego, CA: Academic)

Fishkin J B, Coquoz O, Anderson E R, Brenner M and Tromberg B J 1997 Frequency-domain photon migration measurements of normal and malignant tissue optical properties in a human subject *Appl. Opt.* **36** 10–20

Gandjbakhche A H, Nossal R, Dadmarz R, Schwartzentruber D and Bonner R F 1995 Expected detectability of adenocarcinoma tumors within human breast in time-resolved images *Proc. SPIE* **2387** 111–18

Gullino P M, Jain R K and Grantham F H 1982 Temperature gradients and local perfusion in a mammary carcinoma *J. Natl. Cancer Inst.* **68** 519–31

Jacques S L, Nelson J S, Wright W H and Milner T E 1993 Pulsed photothermal radiometry of port-wine-stain lesions *Appl. Opt.* **32** 2439–46

Jain R K, Grantham F H and Gullino P M 1979 Blood flow and heat transfer in Walker 256 mammary carcinoma *J. Natl. Cancer Inst.* **62** 927–33

Kohl M, Essenpreis M and Cope M 1995 The influence of glucose concentration upon the transport of light in tissue-simulating phantoms *Phys. Med. Biol.* **40** 1267–87

Laufer J 2001 Near-infrared optical coefficients of tumours and adjacent normal tissue *Proc. SPIE Conf. BIOS* (San Jose, 2001)

Long F H and Deutsch T F 1987 Pulsed photothermal radiometry of human artery *IEEE J. Quantum Electron.* **23** 1821–25

Pérennès F, Beard P C and Mills T N 1999 Analysis of a low finesse Fabry–Perot interferometer illuminated by a multimode optical fibre *Appl. Opt.* **38** 7026–34

Prahl S A, Vitkin I A, Bruggemann U, Wilson B C and Anderson R R 1992 Determination of optical properties of turbid media using pulsed photothermal radiometry *Phys. Med. Biol.* **37** 1203–17

Shenfeld O, Eyal O, Goldwasser B and Katzir A 1993 Temperature monitoring and control of CO_2 laser tissue welding in the urinary tract using a silver halide fibre optic radiometer *SPIE Proc.* **1876** 203–14

Troy T L, Page D L and Sevic-Muraca E M 1996 Optical properties of normal and diseased breast tissues: prognosis for optical mammography *J. Biomed. Opt.* **1** 342–55

Valvano J W, Cochran J R and Diller K R 1985 Thermal conductivity and diffusivity of biomaterials measured with self-heated thermistors *Int. J. Thermophys.* **6** 301–11

Wang L-H, Jacques S L and Zheng L-Q 1995 MCML—Monte Carlo modelling of photon transport in multi-layered tissues *Comput. Methods Programs Biomed.* **47** 131–46

Wang L-H, Jacques S L and Zheng L-Q 1997 CONV—Convolution for responses to a finite diameter photon beam incident on multi-layered tissues *Comput. Methods Programs Biomed.* **54** 141–50